Global Space-based Inter-Calibration System

Quarterly

Newsletter Fall 2020 Issue

doi: 10.25923/cfag-b381
Vol. 14 No 3, 2020
Editor: Manik Bali, ESSIC/UMD

CMA • CNES • ESA • EUMETSAT • IMD • ISRO • JAXA • JMA • KMA • NASA • NIST • NOAA • ROSCOSMOS . ROSHYDROMET • SITP • USGS • WMO

Articles

News in This Quarter

Announcements

GSICS Related Publications

Overview of a flexible cross calibration approach for hyperspectral sensors with wide-swath multispectral sensors

By Hiroki Mizuochi (National Institute of Advanced Industrial Science and Technology, Geological Survey of Japan)

Hyperspectral remote sensing enables the in-depth ecological monitoring and exploration of mineral resources. Recently, the International Space Station (ISS) was equipped with various hyperspectral sensors covering the solar reflective spectral domain.

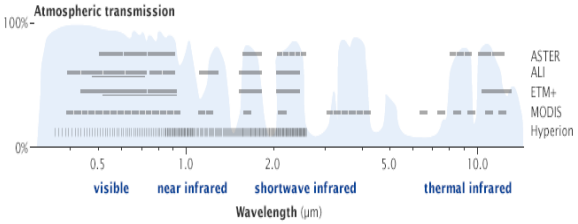

Image above shows the overlapping observing wavelengths of five visible instruments (Image Courtesy of NASA)

Examples are the Hyperspectral Imager Suite (HISUI), and DLR Earth Sensing Imaging Spectrometer (DESIS). If the sensors are radiometrically consistent with each other, the synergetic use of multiple sensors may offer further opportunity for long-term terrestrial monitoring.

Various approaches for cross calibration were developed to improve inter-sensor radiometric consistency. The simplest way of cross calibration is to compare data obtained by different sensors aboard the same satellite platform, viewing the same calibration site at the same time, and over a similar spectral range. However, a satellite platform incorporating multiple comparable sensors is a rarity. Even if multiple sensors are available on the same platform, different sensors generally undertake different observation missions and thus have different spatial and spectral features, making comparison relatively complicated. Further, with regard to hyperspectral cross calibration, inter-band radiometric consistency is not ensured by simply comparing each narrow band between sensors.

Mizuochi et al. (2020) proposed a flexible hyperspectral cross calibration scheme that simultaneously improves inter-sensor and inter-band radiometric consistency [1]. It comprises (1) cross-calibration between analogous bands of a hyperspectral sensor and a well calibrated multispectral reference sensor, and (2) inter-band calibration using the analogous bands of a hyperspectral sensor and a well-calibrated multispectral reference sensor, and (2) inter-band calibration using the corrected analogous bands of the hyperspectral sensor as a reference.

The detailed procedure is shown in Figure 1. To adjust different spectral response between sensors, the linear relationship of surface reflectance between a reference band and a band to be calibrated over a target site (so-called “soil line” [2,3]) must be investigated in advance based on in situ spectral measurement or well-calibrated satellite hyperspectral data. A spatially homogeneous and temporally invariant target is desirable.

doi: 10.25923/cfag-b381

Over the target, the surface reflectance of a reference sensor band is retrieved via the radiative transfer model (RTM) from the top-of-atmosphere (TOA) radiance. The reference surface reflectance is translated by the soil line into surface reflectance in the sensor band to be calibrated and then converted to TOA radiance by the opposite-way RTM. After adjusting the spatial resolution (if necessary), the original TOA radiance in the hyperspectral band can be corrected by the TOA radiance calculated from the reference analogous bands.

The corrected analogous bands in the hyperspectral sensor are regarded as the reference band in the second process, i.e., inter-band calibration. The procedure is almost the same as the first process (i.e., cross calibration between analogous bands): two-way RTM and band translation by the soil line. The difference is that multiple candidates are available as references. Since spectrally adjacent bands tend to show high consistency, the use of two bands spectrally closest to the calibration band (and taking the average of the result) is recommended. After the abovementioned sequent procedures, all the hyperspectral bands are calibrated with reference to the counterpart sensor.

A feasibility study was conducted on open/free hyperspectral data of Hyperion aboard the Earth Observing-1 (EO-1) satellite. Moderate resolution Imaging Spectroradiometer (MODIS) onboard Ter ra was selected as a reference sensor (Table 1) since it is

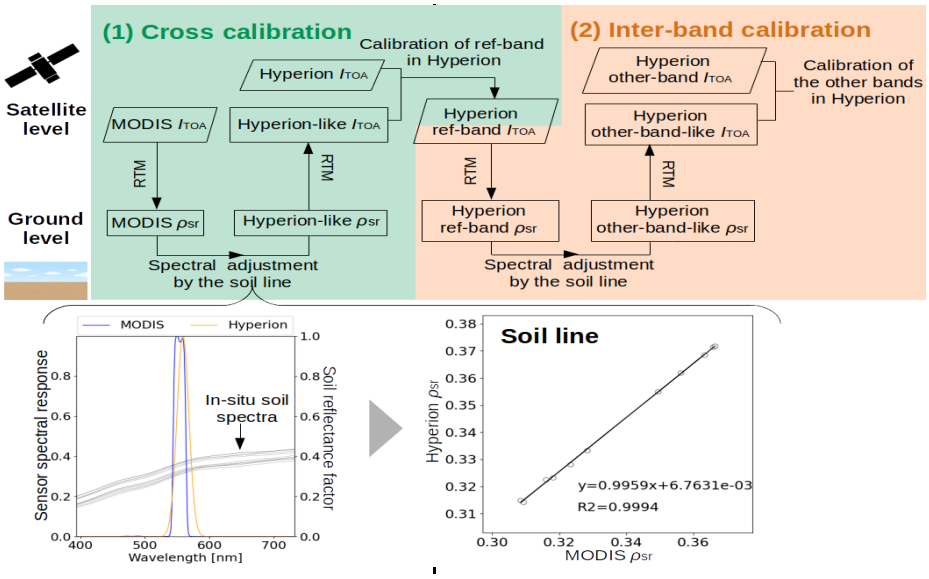

Figure 1. Schematic diagram of the overall procedure and drawing soil lines. Hyperion and MODIS were selected as examples of a hyperspectral sensor to be calibrated and a reference multispectral sensor, respectively. l_{TOA}: TOA irradiance [W/m^2/str], ρ_{sr}: surface reflectance, RTM: radiative transfer model (6SV2.1 was used in the feasibility study).

well calibrated with a wide swath and since Terra follows an orbit similar to EO-1. Totally 18 historical match-up pairs (for 2001–2008) obtained nearly simultaneously with similar sensor and solar geometries were collected. The results for a well-known calibration site, Railroad Valley Playa, Nevada, USA (38.505°N, 115.690°W) showed that the proposed approach can correct not only inter-sensor consistency, but also inter-band consistency, i.e., the spectral continuity in Hyperion TOA radiance was improved (Figure 2). Calibration coefficients to correct the original Hyperion TOA radiance were calculated. They typically ranged 0.9–1.1 with a 0.02–0.04 standard deviation, except for strong atmospheric absorption bands.

Uncertainty in this calibration may arise from MODIS calibration uncertainty, variability under atmospheric conditions input to RTM and RTM algorithm, soil line, geolocation error, and solar irradiance model. According to the sensitivity analysis, the total relative uncertainty of the corrected TOA radiance was estimated as less than 5%. Near the atmospheric absorption bands, the atmospheric condition seems to be a large source of error in inter-band calibration, whereas for the other bands, uncertainty in MODIS reflectance and solar irradiance model were the predominant sources of errors. In addition, since each band of MODIS is independently calibrated, its inter-band consistency should be investigated in future.

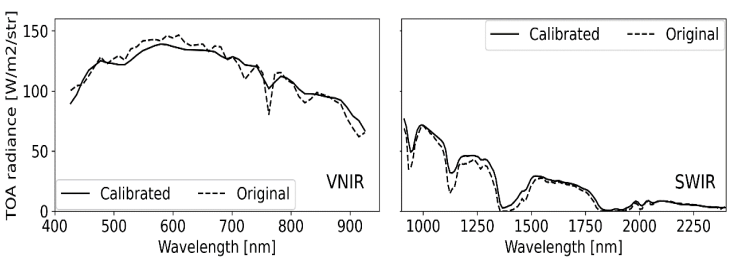

Figure 2. Comparison of the original and the corrected TOA

Band description	MODIS band number and wavelength	Hyperion band number and wavelength
Red	Band 1 (645 ± 25 nm)	Band 29 (640.50 ± 10.32 nm)
Near infrared	Band 2 (858.5 ± 17.1 nm)	Band 50 (854.18 ± 11.28 nm)
Blue	Band 3 (469 ± 10 nm)	Band 12 (467.52 ± 11.39 nm)
Green	Band 4 (555 ± 10 nm)	Band 21 (559.09 ± 10.93 nm)
Short wave infrared 1	Band 5 (1240 ± 10 nm)	Band 110 (1245.36 ± 10.74 nm)
Short wave infrared 2	Band 6 (1640 ± 12 nm)	Band 149 (1638.81 ± 11.50 nm)
Short wave infrared 3	Band 7 (2130 ± 25 nm)	Band 198 (2133.24 ± 10.73 nm)

Table 1 : Analogous bands between Hyperion and MODIS.

doi: 10.25923/cfag-b381

The proposed approach has the potential to realize hyperspectral cross calibration even for irregular-orbit sensors aboard the ISS by searching similar-geometry satellite data at actively monitored and pseudo-invariant calibration sites worldwide. Climate Absolute Radiance and Refractivity Observatory (CLARREO) Pathfinder is one of the candidates, which will be a SI traceable hyperspectral reference on ISS. It is also expected to provide well-calibrated spectra to draw soil lines. Considering the bidirectional reflectance factors, cross calibration with geostationary satellite sensors that offer simultaneous observation with polar- or ISS-orbit sensors is a promising avenue for further application of the proposed approach.

References

[1] Mizuochi, H., Tsuchida, S., Obata, K., Yamamoto, H. and Yamamoto, S., 2020, Combination of cross- and inter-band radiometric calibrations for a hyperspectral sensor using model-based spectral band adjustment. Remote Sens., Vol. 12, No. 12, 2011, DOI:10.3390/rs12122011.

[2] Obata, K., Tsuchida, S. and Iwao, K., 2015, Inter-band radiometric comparison and calibration of ASTER visible and near-infrared bands. Remote Sens., Vol. 7, No. 11, 15140-15160, DOI:10.3390/rs71115140.

[3] Baret, F., Jacquemoud, S. and Hanocq, J.F., 1993, About the soil line concept in remote sensing. Adv. Space Res., Vol. 13, No. 5, 281-284, DOI:10.1016/0273-1177(93)90560-X

TROPOMI in-orbit Earth reflectance validation

By Gijsbert Tilstra, Martin de Graaf, Ping Wang and Piet Stammes (KNMI)

TROPOMI (Tropospheric Monitoring Instrument) onboard ESA's Sentinel-5 Precursor satellite has been collecting data for almost three years now. Daily maps of atmospheric composition with unprecedented detail have been produced. To achieve these results, the level-1 data quality has to get much attention. Detector output is monitored routinely and onboard calibration is applied to maximize the quality of the radiance and irradiance and to correct for instrument degradation.

Here we report the results of an independent study which was setup to estimate the quality of the Earth reflectance measurements. In this study, the Earth reflectances are compared to radiative transfer calculations for clear-sky scenes. This is a technique applied successfully before to other instruments [See Tilstra et al., 2005].

Scenes with clouds and/or large amounts of aerosol are excluded in the study, so the largest source of errors in the radiative transfer calculations is the uncertainty in the surface albedo [Tilstra et al., 2005]. We use the OMI and SCIAMACHY surface Lambertian-equivalent reflectivity (LER) databases [Kleipool et al., 2008; Tilstra et al., 2017] to provide surface albedo input to the simulations. The OMI surface LER database is used for the wavelengths up to 500 nm and the SCIAMACHY surface LER database is used for the longer wavelengths. The calculations were performed by the radiative transfer code DAK ("Doubling-Adding KNMI") for the 21 wavelength bands defined in Table 1. The comparison of the TROPOMI data with the simulations was performed for the period May 2018 till May 2020 by processing one day per fortnight.

Figure 1 presents the results found for the 328-nm wavelength band for 30 October 2019. The green data points represent observations taken over land, the blue data points denote scenes containing water surfaces.

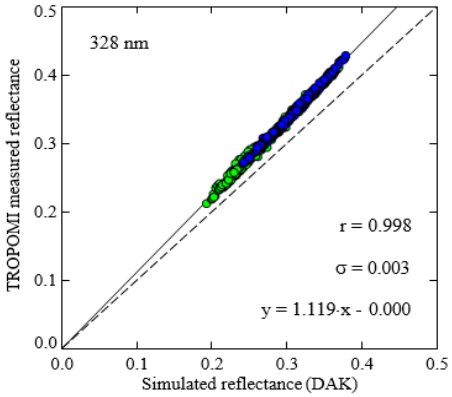

Figure 1: TROPOMI measured reflectance versus DAK simulated reflectance at 328 nm for cloud-free conditions on 30 October 2019. Green circles represent clear-sky scenes over land and blue circles correspond to clear-sky water scenes.

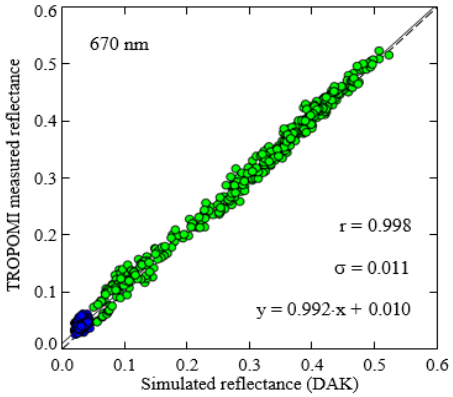

Figure 2: Again, TROPOMI reflectance versus DAK simulated reflectance, but now at 670 nm.

Return to Page One

doi: 10.25923/cfag-b381

Wavelength band (nm)	328	335	340	354	367	380	388	402	416	425	440
Spectral band	3	3	3	3	3	3	3	4	4	4	4
Surface albedo input	OMI	OMI	OMI	OMI	OMI	OMI	OMI	OMI	OMI	OMI	OMI
Percentage $D_{1.0}$	10.1%	8.8%	7.3%	7.4%	7.1%	8.5%	6.7%	6.5%	6.9%	6.5%	6.7%
Wavelength band (nm)	463	494		670	685	697	712	747	758	772	2314
Spectral band	4	4		5	5	5	5	6	6	6	7
Surface albedo input	OMI	OMI		SCIA	SCIA	SCIA	SCIA	SCIA	SCIA	SCIA	SCIA
Percentage $D_{1.0}$	7.0%	6.1%		0.7%	1.0%	0.5%	1.0%	2.2%	2.2%	3.7%	-5.7%

Table 1: Results of the TROPOMI reflectance validation for each of the 21 defined wavelength bands. The percentage $D_{1.0}$ is the estimated calibration error in the TROPOMI reflectance for a case with a reflectance of 1, expressed as a percentage. It was determined for (and over) the entire time period that was studied.

The linear fit through the data points has near zero offset but the slope deviates significantly from one (1.119). The standard deviation of the data points w.r.t. the linear fit is low (σ = 0.003) and Pearson's correlation coefficient r amounts to 0.998. At 328 nm the sensitivity of the reflectance to errors in the surface reflectance is the lowest of all studied 21 wavelength bands. The deviation from the one-to-one relationship in Figure 1 is therefore quite a strong indicator for the existence of errors in the calibration of TROPOMI. In Figure 2, the results for the 670-nm wavelength band are shown. The results are different in the sense that there is now more spread in the data points (σ = 0.011). This is because at this wavelength the reflectance is more sensitive to the uncertainty in the surface albedo input. The linear fit, however, is much closer to the one-to-one relationship. In fact, unlike the 328-nm wavelength band, the 670-nm wavelength band meets the TROPOMI requirements of 2% maximal radiometric error.

Studying the results, we found no dependence on viewing zenith angle, or on any of the other angles, for any of the 21 wavelength bands that were studied. The time dependence was also studied. Trends due to instrument degradation were found, being strongest for the 328-nm wavelength band, almost absent for the 494-nm wavelength band, and virtually absent for the longer wavelengths.

Table 1 summarizes the end results for the validation of the absolute radiometric calibration. The percentage $D_{1.0}$ represents the estimated calibration error in the TROPOMI reflectance for a case with a reflectance of 1, expressed as a percentage. The $D_{1.0}$ was determined over the entire two-year time period that was studied. For most of the wavelength bands in TROPOMI spectral bands 5 and 6 (wavelength bands 670 to 772 nm) the reflectance meets the TROPOMI requirements of maximal error. The exception is the 772-nm wavelength band. Note that the estimated accuracy of the validation method is about 2–3% in this wavelength range.

For the wavelength bands in TROPOMI spectral bands 3 and 4 (wavelength bands 328 to 494 nm), we find, depending on the wavelength, differences $D_{1.0}$ to lie between 6% and 10%. The differences are much larger than the estimated accuracy of the method (1–3%), and therefore significant. It should be noted that the magnitude of the errors agrees with radiometric calibration errors found recently in the TROPOMI solar irradiance product [Ludewig et al., 2020, Fig. 20]. We conclude that for spectral bands 3 and 4 the radiometric calibration does not meet the TROPOMI calibration requirements. Work is ongoing to improve the calibration for the next version of the data.

The 2314-nm wavelength band in TROPOMI spectral band 7 also does not meet the requirements. Moreover, for this wavelength band an unexplained seasonal variation in the calibration error was found. More information on the approach that was followed and the results can be found in Tilstra et al. [2020]. The work will be continued to monitor instrument degradation and to investigate long-term trends.

References

Kleipool, Q. L., et al.:, Earth surface reflectance climatology from 3 years of OMI data, J. Geophys. Res., 113, D18308, doi:10.1029/2008JD010290, 2008.

Ludewig, A., et al.:, In-flight calibration results of the TROPOMI payload on board the Sentinel-5 Precursor satellite, Atmos. Meas. Tech., 13, 3561–3580, doi:10.5194/amt- 13-3561-2020, 2020.

Tilstra, L. G et al.:, Method for in-flight satellite calibration in the ultraviolet using radiative transfer calculations, with application to Scanning Imaging Absorption Spectrometer for Atmospheric Chartography (SCIAMACHY), J. Geophys. Res., 110, D18311, doi:10.1029/2005JD005853, 2005.

Tilstra, L. G.:, et al.:, Surface reflectivity climatologies from UV to

doi: 10.25923/cfag-b381

NIR determined from Earth observations by GOME-2 and SCIAMACHY, J. Geophys. Res.-Atmos., 122, 4084–4111, doi:10.1002/2016JD025940, 2017.

Tilstra, L. G. et al.:, In-orbit Earth reflectance validation of TROPOMI on board the Sentinel-5 Precursor satellite, Atmos. Meas. Tech., 13, 4479–4497, doi:10.5194/amt-13-4479-2020, 2020

Calibration and Validation Activities for the PAZ Polarimetric Radio Occultation and Heavy Precipitation (ROHP-PAZ) experiment

By Ramon Padullés (ICE-CSIC, IEEC), Estel Cardellach (ICE-CSIC, IEEC), Chi O. Ao (JPL/Caltech), F. Joe Turk (JPL/Caltech), Kuo-Nung Wang (JPL/Caltech), Manuel de la Torre Juárez (JPL/Caltech), and Byron Iijima (JPL/Caltech)

The Radio Occultation and Heavy Precipitation experiment on the Spanish PAZ satellite (ROHP-PAZ) was activated on May, 2018. The aim of the experiment was to demonstrate the sensitivity of Polarimetric Radio Occultations (PRO) to heavy precipitation events [1]. Such a goal was rapidly achieved, with polarimetric observables showing significant positive values when obtained within heavy precipitating systems [2]. However, careful calibration was required in order to mitigate and assess non-precipitation effects [3].

PRO enhances the standard GNSS-RO technique by measuring the GNSS signals in two orthogonal linear polarizations (horizontal and vertical) instead of a single right-hand circular polarization (RHCP). The PRO observable is the difference between the excess phase simultaneously measured at the two polarizations ($\Delta\phi = \phi_H - \phi_V$). Heavy precipitation along the occultation rays induces a positive difference between the delays of the horizontal and the vertical components of the electromagnetic field, due to the asymmetry of falling flattened hydrometeors (such as raindrops). The PRO instrument is designed to precisely measure this phase difference.

The contribution from hydrometeors must be isolated from other effects, in order to quantify its effect and relate it to geophysical parameters such as rain rate or water content. The on-orbit calibration of the PRO experiment was focused on assessing the effect of (1) a metallic structure installed near the polarimetric antennae; and (2) the ionospheric Faraday Rotation. In order to perform the calibration, all PRO observations were co-located with the precipitation retrievals from the GPM IMERG products [4], and the inter-calibrated infrared brightness temperature from the NCEP-CPC [5]. Information about the ionosphere was obtained through the IGRF Earth's magnetic field model (*https://www.ngdc.noaa.gov/IAGA/vmod/igrf.html*) and the IRI model for the electron density (*http://irimodel.org/*).

The PAZ observations were grouped by different thresholds of precipitation and ionospheric activity. Using the data obtained in non-precipitating areas and under low ionospheric conditions, an on-orbit antenna pattern was built. Note that the auxiliary data are only used for grouping the PAZ observations in the calibration process, not for adjusting the observables.

The metallic structure sitting next to and partially over the antenna induces a strong multipath pattern, and part of the field of view is blocked. In Fig.1, we show the on-orbit estimated antenna patterns for the Signal to Noise Ratio (SNR) at H and V (panels (a) and (b)), and for the $\Delta\phi$ (panel (c)).

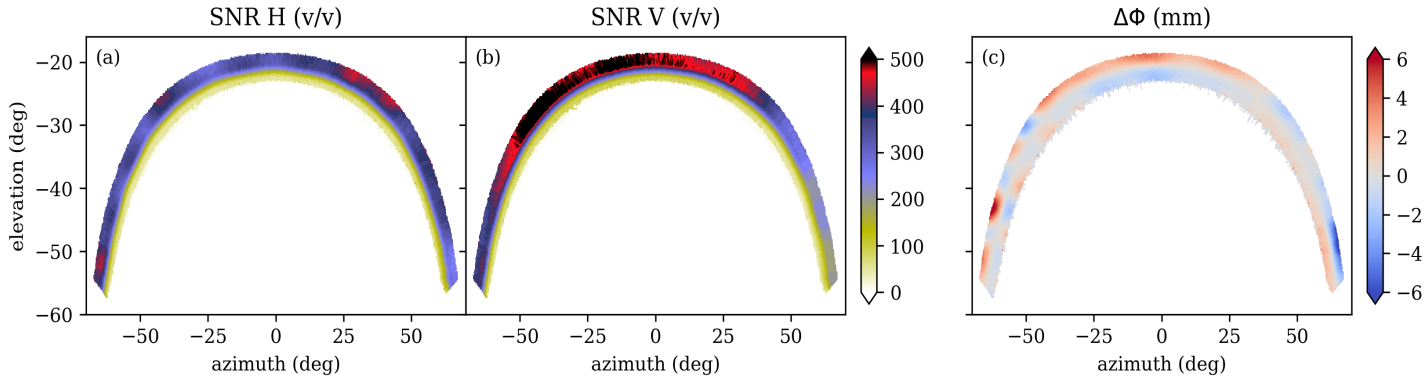

Figure 1. On-orbit antenna pattern using observations collected in non-precipitating areas and under low ionospheric activity. See *[3]* for further details on the coordinate system. (a), (b) and (c) are the antenna patterns for the SNR H, V and the $\Delta\phi$ observable, respectively.

doi: 10.25923/cfag-b381

These antenna patterns are constructed as a function of the azimuth and the elevation, as seen from the point of view of the antenna [3].

The antenna H, which was designed to perform better than V, exhibits an SNR pattern that fluctuates along the azimuth direction, caused by multipath and near field effects. The SNR pattern for the V antenna shows a shift towards negative azimuths of its maximum performance, and a steep drop of SNR for azimuths > 50 deg. These features translate into an irregular Δϕ pattern.

The antenna pattern for Δϕ is used to calibrate all Δϕ observations by subtracting the pattern from the observations. This ensures that systematic effects present regardless of the precipitation are seamlessly corrected for all observations. Potential residual effects from the ionosphere are further corrected by subtracting a linear fit obtained in the upper layers of the observations, where no hydrometeors are expected [6]. The effect of the ionosphere has been found to be very small, and no significant trend with ionospheric activity is observed.

The results of the calibration are validated against the IMERG precipitation retrievals. In Figure 2, panel (a), we show in black the mean of the Δϕ as a function of height (time observations are mapped to height using geometric optics), for all the cases where no precipitation is sounded according to IMERG. The orange shade represents its standard deviation. The standard deviation is 1.5 mm at 2km, and improves with altitude (it is 1 mm at 3km, and it is better than 0.5mm

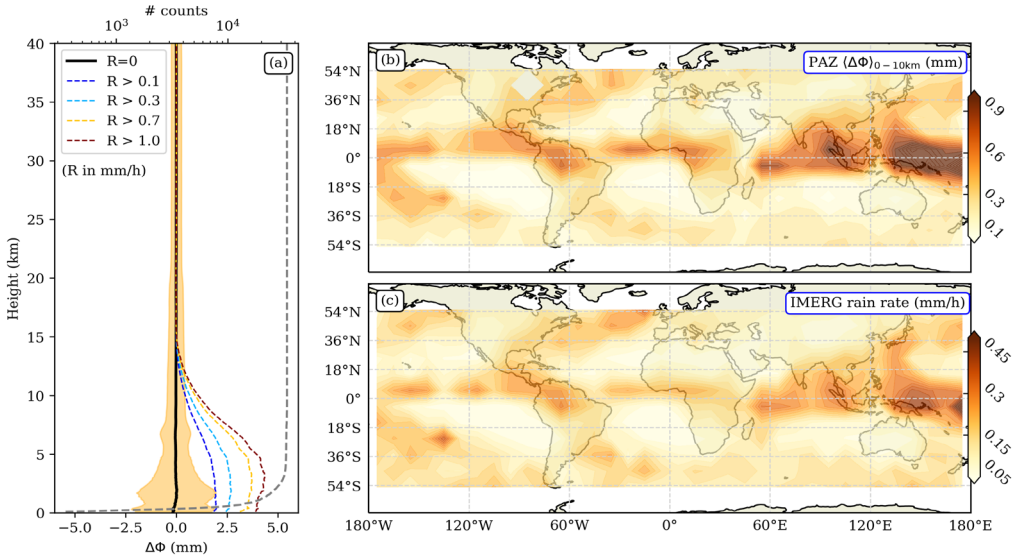

Figure 2. Validation of the on-orbit calibration. (a) Averaged Δϕ as a function of height for all the cases with no rain (black) and rain above a certain threshold (dashed colored lines, see legend). The gray dashed line ruled by the top axis show the number of no-rain profiles included in the average. (b) and (c) show the 10ºx10º averaged $<\Delta\phi>_{0\text{-}10km}$, and IMERG rain rate, respectively.

above 10km). These numbers agree with the pre-launch studies [1]. When the data is grouped by different precipitation thresholds, the mean increases with increasing precipitation (dashed colored lines). To further validate the measurement, the average Δϕ between 0 and 10 km, $<\Delta\phi>_{0\text{-}10km}$ (so that it acts as a representative single value of each observation), is compared with IMERG precipitation. All observations are averaged over a grid of 10º x 10º and shown in panels (b) and (c) of Figure 2. It can be seen how Δϕ captures the well-known spatial patterns of precipitation remarkably well.

These results show successful on-orbit calibration of the Δϕ observable for PRO. Δϕ exhibits a clear positive relationship with the presence and intensity of precipitation, showing the potential of Δϕ for precipitation studies. Specially, when it is combined with the thermodynamic products retrieved from the same dataset as any other standard RO mission. The data can be downloaded from *https://paz.ice.csic.es/* and will also be available at *https://genesis.jpl.nasa.gov*.

References:

[1] Cardellach, E., et al., 2014, doi:10.1109/TGRS.2014.2320309.

[2] Cardellach, E., et al., 2019, doi:10.1029/2018GL080412.

[3] Padullés, R., et al., 2020, doi:10.5194/amt-13-1299-2020.

[4] Huffman, G.J., et al., 2019, doi:10.5067/GPM/IMERG/3B-HH/06.

[5] Janowiak, J., et al., 2017, doi:10.5067/P4HZB9N27EK

[6] Tomás, S., et al., 2018, doi:10.1109/TGRS.2018.2831600.

The research by the US authors was carried out at the JPL/Caltech under a contract with NASA.

doi: 10.25923/cfag-b381

A Deep Learning Trained Clear-Sky Mask Algorithm for VIIRS Radiometric Bias Assessment

By Xingming Liang (UMD) and Quanhua (Mark) Liu (NOAA)

Monitoring sensor radiometric biases is a key component of the Global Space-based Inter-Calibration System (GSICS, gsics.wmo.int) [1] and A clear-sky mask (CSM) is critical to improve the radiometric biases.

The NOAA Integrated Calibration and Validation System Long-Term Monitoring (ICVS, https://www.star.nesdis.noaa.gov/icvs) [2] is a typical examples used to monitor sensor radiometric biases in clear-sky conditions with the community radiative transfer model (CRTM) [3] as a reference. The CSM algorithms are customarily based on the radiative characteristics of various cloud formations, and use massive empirical thresholds together with multi-tests under various spatial and temporal conditions combined with sensor measurements to achieve clear-sky identification [4]. However, the complicated physical-based CSM algorithms are computationally consuming and the empirical thresholds are very dependent on the specific sensor to be utilized, resulting in the need to re-test and re-design for each new sensor. With the new generation sensors, such as the Visible Infrared Imaging Radiometer Suite (VIIRS) onboard the satellites in the Joint Polar Satellite System (JPSS), the efficiency of CSM algorithms is a key issue for the real-time monitoring of the sensor radiometric biases in global clear-sky condition.

With the evolution of artificial intelligence (AI), the approach used in artificial neural networks (ANN) has gradually applied in most science and technical fields, including atmosphere and ocean remote sensing [5]. A fully connected deep neural network (FCDN) algorithm applied for VIIRS clear-sky mask (FCDN_CSM) [6] has been developed that efficiently identifies clear-sky pixels for real-time monitoring of the VIIRS observation minus CRTM simulation (O-M) biases for five thermal emission M bands (TEB/M). The FCDN_CSM architecture constitute two hidden layers and 10 input features, including TEB/M brightness temperatures (BT), senor geophysical parameters, and atmosphere and surface ancillary data, extracted from the European Centre for Medium-Range Weather Forecasts (ECMWF, https://www.ecmwf.int) and Canadian Meteorology Centre (CMC) SST product https://podaac.jpl.nasa.gov/dataset/CMC0.1deg-CMC-L4-GLOB-v3.0). Four CSM types from the advanced clear-sky processor over ocean (ACSPO) CSM [4] were used as labels. The model was trained by VIIRS data from March 1-10, 2019, together with the ancillary data. The well-trained FCDN_CSM were then used/ to predict CSM for later-on several days as an accuracy and stability check.

The prediction results indicated that: 1) FCDN_CSM has high prediction accuracy. Table 1 shows the most accuracy is type Cloud, where recall and precision reach 96.6% and 98.5%, respectively, following by Clear-Sky for BT (CS_BT), are 93.76% and 92.70%. The global O-M mean biases and standard deviation (STD) by using FCDN_CSM are comparable with the ACSPO version 2.40. Figure 1 upper panels show global distribution of CSM types for S-NPP VIIRS are comparable between ACSPO and FCDN_CSM. 2) FCDN_CSM has migration advantage. Figure 1 bottom panels show the global distribution of CSM types for NOAA-20 are also comparable with CSPO, where the FCDN_CSM was trained by the S-NPP data. This indicated that the S-NPP data trained FCDN-CSM could apply for NOAA-20 without significant accuracy loss, and is outperform traditional CSM model, which is dependent on the specific sensor. This migration advantage suggested that the FCDN_CSM could be a potential proxy CSM for the calibration and validation of the newly VIIRS onboard the follow-up JPSS satellites before the physics-based CSM is available. 3) FCDN_CSM has high efficiency. Using NOAA internal Linux server with 100 G memory and 2.2 G multi-core CPUs and without GPU support, FCDN-CSM takes less than one minute to generate one day of CSM (about 0.6 billion pixels), and is also superior to the time-consuming traditional CSM which takes several hours to generate the same size of the CSM data.

4) FCDN_CSM has short-term stability. Figure 3 shows the O-M error

	SNPP			
	ACSPO N	ML N	Recall (%)	Precision (%)
CS_BT	3348	3139	93.76	92.70
PCS	703	674	95.87	86.19
CLOUD	15575	15050	96.63	98.52
CS_SST	374	330	88.24	80.29
ALL	20000	19193	95.97	96.67

Table 1. The recalls and precisions of the test dataset of four CSM data types.

doi: 10.25923/cfag-b381

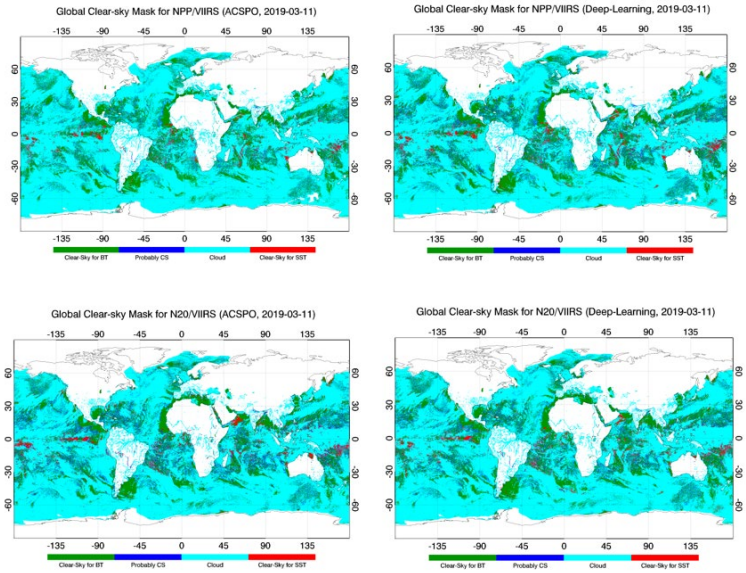

Figure 1. Global distribution of the four CSM types from ACSPO (left) and FCDN-CSM (right) for S-NPP (upper) and NOAA-20 (bottom)

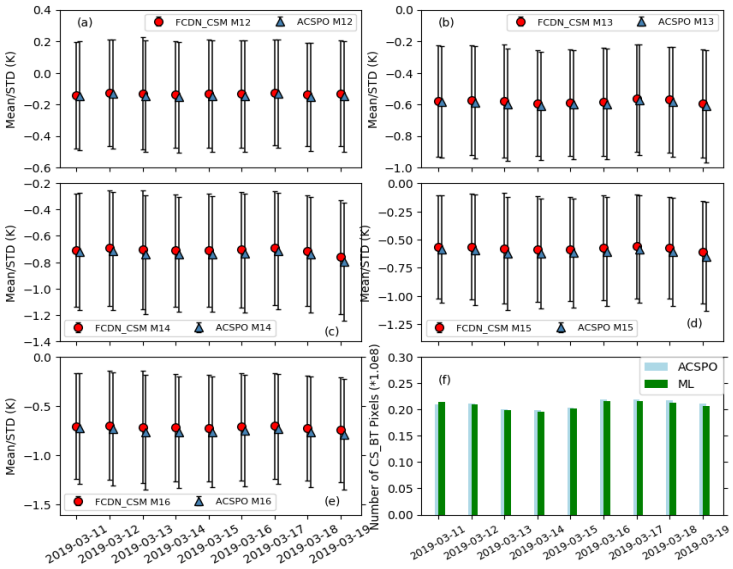

Figure 2. The M-O mean and STD error bars by using ACSPO CSM and FCDN_CSM for nine-day data from March 11 to 19, 2019 for (**a**) M12, (**b**) M13, (**c**) M14, (**d**) M15, and (**e**) M16, and corresponding NCSPs (**f**).

bars with STDs for five TEB/M bands from March 11–19, 2019, by using ACSPO CSM and FCDN-CSM prediction. The O-M mean, STDs, and number of clear-sky pixels (NCSP) were stable and comparable with ACSPO in all bands and all days.

The differences of the mean and STDs were within 0.01 ± 0.02 K, and the NCSP differences were less than 0.5%, indicating that the FCDN-CSM model is stable and can work well for a short-term period. The further improvement to long-term stability has been analyzed and the new model is referred as FCDN_CSM version 2, and the document of this work is currently under review on the Journal of Remote Sensing. Overall, the FCDN_CSM advantages suggested that the model could be a potential proxy CSM for VIIRS to identify clear-sky domain accurately and efficiently, and improve VIIRS radiometric biases.

References

[1] Goldberg, M., G. Ohring, J. Butler, C. Cao, R. Datla, D. Doelling, et al., "The global space-based inter-calibration system," Bulletin of the American Meteorological Society, vol. 92, pp. 467-475, Apr 2011

[2] Liang, X., Sun, N., Ignatov, A., Liu, Q., Wang, W., Zhang, B., Weng, F., Cao, C. Monitoring of VIIRS ocean clear-sky brightness temperatures against CRTM simulation in ICVS for TEB/M bands," Proc. SPIE 10402, Earth Observing Systems XXII, 2017, 104021S, doi: 10.1117/12.2273443

[3] Liu, Q., Boukabara, S. Community Radiation Transfer Model (CRTM) Applications in Supporting the Suomi National Polar-Orbiting Partnership (SNPP) Mission validation and Verification, Remote Sen. Environ., 2014 140, 744-754

[4] Petrenko, B., Ignatov, A., Kihai, Y., Heidinger, A. Clearsky mask for the Advanced Clear-Sky Processor for Oceans. *J. Atmos. Ocean. Technol.* **2010**, *27*, 1609–1623.

[5] Boukabara, S. A., Maddy, E., Shahroudi, N., Hoffman, R. N., Connor, T. Artificial Intelligence (AI) Techniques to Enhance Satellite Data Use for Nowcasting and NWP/Data Assimilation. 100th American Meteorological Society Annual Conference, Boston, 2020

[6] Liang, X., Liu, Q., Yan, B., Sun, N. A Deep Learning Trained Clear-Sky Mask Algorithm for VIIRS Radiometric Bias Assessment. *Remote Sens.* 2020, *12*, 78.

doi: 10.25923/cfag-b381

NEWS IN THIS QUARTER

The ESA atmospheric Validation Data Centre (EVDC): the portal updates

By Paolo Castracane[1], Angelika Dehn[2], Jarek Dobrzanski[3], Ann Mari Fjaeraa[4], Paul Kiernan[3] and Alastair McKinstry[5] [1]RHEA System S.p.A c/o ESA/ESRIN; [2]ESA/ESRIN; [3]Skytek; [4]NILU; [5]ICHEC

Introduction

The ESA atmospheric Validation Data Centre (EVDC) is the official ESA repository for calibration and validation (Cal/Val) data, it provides an online information system supporting users to exploit campaign datasets for Earth Observation missions and applications in the atmospheric domain. The EVDC portal (https://evdc.esa.int/) offers several tools for Cal/Val data query, data upload/download, format conversion (GEOMS conversion routines), orbital prediction (to generate, visualize and download satellite's instrument overpass and to plan campaign measurements) and for production of ECMWF parameter's maps. It also provides an access to satellite data for specific missions, in particular for the new atmospheric composition/dynamic missions, namely Sentinel-5P, and, in the near future, Aeolus. The portal can be easily expanded to support new campaigns and satellite missions. Data exchange with the EVDC is regulated by a protocol with the aim to ensure data ownership, to prevent re-distribution to third parties and to protect intellectual properties.

The recent EVDC portal updates have been applied to the following main items:

1. Access to full archive of Sentinel 5P products.
2. Cal/Val search capabilities.
3. Online GEOMS file generator.
4. Orbit Prediction Tool.
5. Processing capabilities.
6. Data Interoperability.

Access to Full Archive of Sentinel 5P Products

EVDC provides registered user with an access to daily updated archives of Sentinel 5P level2 data. Users can query the products using many advanced filters and download them or save their search results and schedule bulk processing jobs online using commands provided by the HARP tool [1] and bulk download the processing results.

Cal/Val Search Capabilities

The EVDC repository includes a large variety of data from: campaigns, networks, in-situ ground-based measurements, aircraft, balloons and, in general, from a wide range of stations and measurements principles. The Cal/Val search facility allows users to use an interactive map when searching for correlative data and offers better speed and integrity of search terms.

The help system and tooltips explaining the meaning of each field and linking to the relevant documentation in the portal make Cal/Val data search more accessible.

Figure 1 EVDC Portal home page

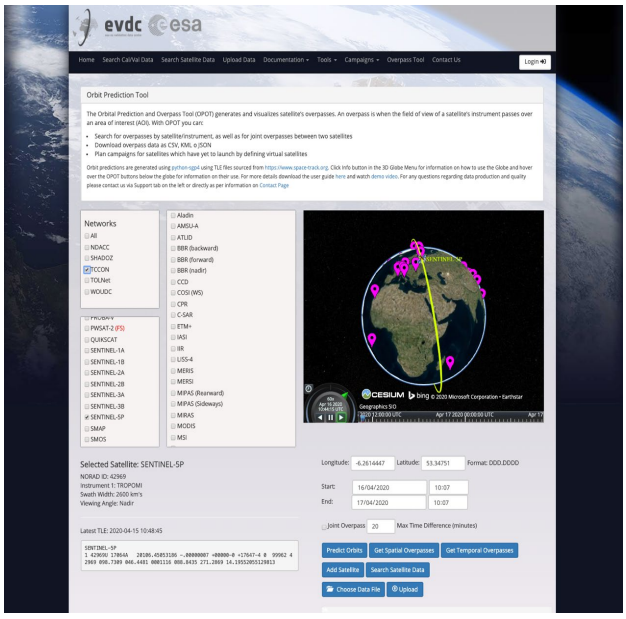

Figure 2 EVDC Orbit Prediction Overpass Tool

doi: 10.25923/cfag-b381

Online GEOMS File Generator

As part of our effort to support standardization of correlative data formats, an online tool has been developed with the aim to generate GEOMS file(s) (formatted as HDF4, HDF5 or netCDF) as output. The tool supports user to prepare specific metadata templates that are required, together with an asci data, as input.

Orbit Prediction Overpass Tool

The Orbit Predictor Overpass Tool (OPOT) exploits the TLEs (Two-Line Element set) as input for each satellite and the Simplified General Perturbation Model (SGP4) [2] to predict and store their future orbits. With OPOT you can:

- Search for overpasses by satellite/instrument, as well as for joint overpasses between two satellites;
- Download overpass data as CSV, KML or JSON;
- Exploit OPOT integration with the Cal/Val database;
- Visualize locations of ground networks on 3D Globe and detailed information about the station;
- Plan campaigns for satellites which have yet to launch by defining virtual satellites.

Processing Capability

The EVDC online data processing capabilities have been migrated to ICHEC infrastructure (Kay supercomputer), where it operates on "Cluster" type nodes allowing for faster and more parallelized execution of processing improving scalability and potential of the system.

In support of the satellite archive, a processing interface has been developed to streamline and simplify workflows related to satellite products using the cloud infrastructure. Users can save their search results and catalogue product bundles and then use these bundles as an input for processing jobs. They can, also, store and reuse frequently used types of HARP Operations. The jobs scheduled for bundles of products are called Orders. Each Order can be converted into a Systematic Order which means the same search criteria will be applied to the future products and the results systematically delivered through email notifications.

Data Interoperability

EVDC is connected to other archives through data interoperability technologies. In order to facilitate simpler and faster search methods for the users, EVDC is setting up harvesting methods for sharing metadata among data archives from a number of national and international projects and programs. Through metadata sharing, EVDC aims to encourage cooperation between the various archives, promote open data policy and strengthen collaboration throughout EO disciplines in the best possible way.

More information about the metadata sharing, the OAI-PMH technique and "behind-the-scenes" information can be found in the portal [3]. To register your archive in this initiative and to set up the required protocols, please contact the EVDC team (nadirteam@nilu.no).

Support and contacts

After initial tests of the updated platform performed by scientists involved in Cal/Val projects, it became clear that more contextual help and documentation references need to be provided. The contextual help hint system was developed and some more references provided in several areas of the portal. However, the EVDC team is available for support, hereafter the team involvement and responsibilities.

NILU: Ann Mari Fjaeraa, Project leader of the NADIR/EVDC system. Main responsibilities: Cal/Val data, Metadata harvesting, GEOMS tools
Contact: nadirteam@nilu.no

Skytek: Paul Kiernan, CTO; Jarek Dobrzanski, Software Engineer
Contact: jarek.dobrzanski@skytek.com

ICHEC: Alastair McKinstry
info@ichec.ie

ESA/ESRIN: Paolo Castracane: Paolo.Castracane@esa.int and Angelika Dehn: Angelika.Dehn@esa.int;

References

[1] https://atmospherictoolbox.org/harp/

[2]www.celestrak.com/NORAD/documentation/spacetrk.pdf

[3]https://evdc.esa.int/documentation/oai-pmh/

doi: 10.25923/cfag-b381

Ken Holmlund (GSICS EP Vice Chair) joins WMO as Head of Space Systems and Utilization

By Manik Bali (ESSIC/UMD)

In the fall of 2020 after 25 years at EUMETSAT where he last served as Chief Scientist, Dr Ken Holmlund moved to WMO as Head of Space Systems and Utilization.

Ken has served the GSICS community for over a decade, most recently (since 2014) as the Vice Chair of GSICS Executive Panel.

Dr Holmlund started his career in satellite remote sensing at the Finnish Meteorological Institute in 1986. In 1989 he joined the European Space Agency to work on the Meteosat satellite programme, focusing on development of products and applications from geostationary satellite data. In 1995 he moved to EUMETSAT to work on the Meteosat Second Generation programme from where he subsequently moved to the Operations Department within EUMETSAT as Head of the Meteorological Operations Division in 2002.

In January 2013, Dr Holmlund became the Head of the newly formed Remote Sensing and Products Division within the Technical and Scientific Support Department in EUMETSAT. In this role, he was responsible for centrally performed scientific developments targeting the extraction of Level-1 and Level-2 data from all instruments on the EUMETSAT missions. He was also responsible for calibration and quality aspects of the EUMETSAT instruments data, which combined with his experience from product operations, constituted a valuable input to the GSICS activities.

Dr. Holmlund has published numerous articles on remote sensing. In addition to his support of GSICS, he has served as a member of several committees including the AMS Committee on Satellite Meteorology, Oceanography, and Climatology, WMO Polar Satellite Task Group, THORPEX Observation Panel, GCOS AOPC, ECMWF Technical Advisory Committee and the

Dr. Ken Holmlund

EUMETNET Science and Technology Advisory Committee.

GSICS would like to thank Dr. Holmlund for the huge contribution he has made as a member of the Executive Panel and in leadership as the Vice Chair. His guidance has prepared us to meet the coming challenges. We look forward to continued support in his new role as a member of the WMO secretariat.

Announcements

GSICS Annual Meeting 2021 to be held via webex

By Dohyeong Kim (KMA) and Lawrence E. Flynn (NOAA)

The 2021 GSICS Joint Meeting for Research and Data Working Groups will be organized as a comprehensive multi-day web meeting. This multi-day web meeting will be held on dates between mid March 2021 through April 2021.Meeting details and agendas will be discussed and arranged over the next two months.

doi: 10.25923/cfag-b381

Call for SPIE Optics and Photonics Earth Observing Systems XXVI conference to be held in San Diego Aug 1-5, 2021

By Jim Butler (NASA), Xiaoxiong (Jack) Xiong (NASA) and Xingfa Gu (Institute of Remote Sensing and Digital Earth, CAS)

The annual SPIE Optics and Photonics' Earth Observing Systems XXVI Conference will be held August 1-5, 2021 at the San Diego Convention Center, San Diego, CA.

The Earth Observing Systems XXVI conference welcomes the submission of papers over a wide range of remote sensing topics. Papers are solicited in the following general areas:

SPIE. The international society for optics and photonics

- Earth-observing mission studies including new system requirements and plans
- commercial system designs
- electro-optical sensor designs and sensitivity studies
- ultraviolet through thermal infrared, microwave, radar, and lidar remote sensing systems
- hyperspectral remote sensing instruments and methodologies
- instrument sub-system and system level pre-launch and on-orbit calibration and characterization
- vicarious calibration techniques and results
- satellite instrument airborne simulators
- techniques for enhancing data processing, reprocessing, archival, dissemination, and utilization
- conversion from research to operational systems
- on-orbit instrument inter-comparison techniques and results
- enabling technologies (optics, antennas, electronics, calibration techniques, detectors, and models)
- sensor calibration traceability, uncertainty, and pre-launch to on-orbit performance assessments
- lunar radiometry and photometry
- remote sensing data acquisition and analysis.

The conference call for papers is available online at https://spie.org/OPO/conferencedetails/earth-observing-systems?SSO=1
Conference abstracts are due February 3, 2021, and proceedings manuscripts are due July 7, 2021

GSICS-Related Publications

Bhatt, Rajendra, David R. Doelling, Conor Haney, Douglas A. Spangenberg, Benjamin Scarino, and Arun Gopalan. 2020. 'Clouds and the Earth's Radiant Energy System Strategy for Intercalibrating the New-Generation Geostationary Visible Imagers'. *JOURNAL OF APPLIED REMOTE SENSING* 14 (3). https://doi.org/10.1117/1.JRS.14.032410.

Carminati, Fabien, Nigel Atkinson, Brett Candy, and Qifeng Lu. 2020. 'Insights into the Microwave Instruments Onboard the Feng-Yun 3D Satellite: Data Quality and Assimilation in the Met Office NWP System'. *ADVANCES IN ATMOSPHERIC SCIENCES*. https://doi.org/10.1007/s00376-020-0010-1.

Fiolleau, Thomas, Remy Roca, Sophie Cloche, Dominique Bouniol, and Patrick Raberanto. 2020. 'Homogenization of Geostationary Infrared Imager Channels for Cold Cloud Studies Using Megha-Tropiques/ScaRaB'. *IEEE TRANSACTIONS ON GEOSCIENCE AND REMOTE SENSING* 58 (9): 6609–22. https://doi.org/10.1109/TGRS.2020.2978171.

Helder, Dennis, Cody Anderson, Keith Beckett, Rasmus Houborg, Ignacio Zuleta, Valentina Boccia, Sebastien Clerc, Michele Kuester, Brian Markham, and Mary Pagnutti. 2020. 'Observations and Recommendations for Coordinated Calibration Activities of Government and Commercial Optical Satellite Systems'. *REMOTE SENSING* 12 (15). https://doi.org/10.3390/rs12152468.

Helder, D., D. Doelling, R. Bhatt, T. Choi, and J. Barsi. 'Calibrating Geosynchronous and Polar Orbiting Satellites: Sharing Best Practices'. *Remote Sensing* 12, no. 17 (2020). https://doi.org/10.3390/RS12172786.

Return to Page One

Hu, Xiuqing, Ling Wang, Junwei Wang, Lingli He, Lin Chen, Na Xu, Bingcheng Tao, Lu Zhang, Peng Zhang, and Naimeng Lu. 2020. 'Preliminary Selection and Characterization of Pseudo-Invariant Calibration Sites in Northwest China'. *REMOTE SENSING* 12 (16). https://doi.org/10.3390/rs12162517.

Yan, B., J. Chen, C.-Z. Zou, K. Ahmad, H. Qian, K. Garrett, T. Zhu, D. Han, and J. Green. 'Calibration and Validation of Antenna and Brightness Temperatures from Metop-C Advanced Microwave Sounding Unit-A (AMSU-A)'. *Remote Sensing* 12, no. 18 (2020). https://doi.org/10.3390/RS12182978.

Yang, W., H. Meng, R.R. Ferraro, and Y. Chen. 'Inter-Calibration of AMSU-A Window Channels'. *Remote Sensing* 12, no. 18 (2020). https://doi.org/10.3390/RS12182988.

Ye, Xin, Xiaolong Yi, Chao Lin, Wei Fang, Kai Wang, Zhiwei Xia, Zhenhua Ji, Yuquan Zheng, De Sun, and Jia Quan. 'Instrument Development: Chinese Radiometric Benchmark of Reflected Solar Band Based on Space Cryogenic Absolute Radiometer'. *REMOTE SENSING* 12, no. 17 (September 2020). https://doi.org/10.3390/rs12172856.

Submitting Articles to the GSICS Quarterly Newsletter:

The GSICS Quarterly Press Crew is looking for short articles (800 to 900 words with one or two key, simple illustrations), especially related to calibration / validation capabilities and how they have been used to positively impact weather and climate products. Unsolicited articles may be submitted for consideration anytime, and if accepted, will be published in the next available newsletter issue after approval / editing. Please send articles to manik.bali@noaa.gov.

With Help from our friends:

The GSICS Quarterly Editor would like to thank Tim Hewison (EUMETSAT), Cheng-Zhi Zou (NOAA), David R. Doelling (NASA) and Lawrence Flynn (NOAA) for reviewing articles in this issue. Thanks are due to Jan Thomas (NOAA) for critical help on 508 compliance

Published By

GSICS Coordination Center
NOAA/NESDIS/STAR NOAA
Center for Weather and Climate Prediction,
5830 University Research Court
College Park, MD 20740, USA

CISESS
5825 University Research Court, Suite 4001,
University of Maryland, College Park, MD 20740-3823